

## Polyethylene glycol-coated blue-emitting silicon dots with improved properties for uses in aqueous and biological environments

This content has been downloaded from IOPscience. Please scroll down to see the full text.

2016 Nanotechnology 27 475704

(<http://iopscience.iop.org/0957-4484/27/47/475704>)

View [the table of contents for this issue](#), or go to the [journal homepage](#) for more

### Download details:

IP Address: 207.162.240.147

This content was downloaded on 25/10/2016 at 15:03

Please note that [terms and conditions apply](#).

You may also be interested in:

[Poly\(D, L-lactide-co-glycolide\) nanoparticles as delivery agents for photodynamic therapy: enhancing singlet oxygen release and phototoxicity by surface PEG coating](#)

Ester Boix-Garriga, Pilar Acedo, Ana Casadó et al.

[Colloidal silicon quantum dots: synthesis and luminescence tuning from the near-UV to the near-IR range](#)

Batu Ghosh and Naoto Shirahata

[Upconverting crystal/dextran-g-DOPE with high fluorescence stability for simultaneous photodynamic therapy and cell imaging](#)

HanJie Wang, Sheng Wang, Zhongyun Liu et al.

[Silicon nanoparticles: Preparation, properties, and applications](#)

Chang Huan and Sun Shu-Qing

[Functionalization of emissive conjugated polymer nanoparticles by coprecipitation: consequences for particle photophysics and colloidal properties](#)

Amita Singh, Michael Bezuidenhout, Nichola Walsh et al.

[Highly surface functionalized carbon nano-onions for bright light bioimaging](#)

Marco Frasconi, Viviana Maffei, Juergen Bartelmess et al.

# Polyethylene glycol-coated blue-emitting silicon dots with improved properties for uses in aqueous and biological environments

Damián Rodríguez Sartori<sup>1</sup>, Cristian R Lillo<sup>1</sup>, Juan J Romero<sup>1</sup>,  
María Laura Dell'Arciprete<sup>1</sup>, Alejandro Miñán<sup>1</sup>,  
Mónica Fernández Lorenzo de Mele<sup>1,2</sup> and Mónica C Gonzalez<sup>1</sup>

<sup>1</sup>Instituto de Investigaciones Fisicoquímicas Teóricas y Aplicadas (INIFTA), Facultad de Ciencias Exactas, Universidad Nacional de La Plata, Casilla de Correo 16, Suc. 4, (1900) La Plata, Argentina

<sup>2</sup>Facultad de Ingeniería, Universidad Nacional de La Plata, (1900) La Plata, Argentina

E-mail: [gonzalez@inifta.unlp.edu.ar](mailto:gonzalez@inifta.unlp.edu.ar)

Received 19 April 2016, revised 23 September 2016

Accepted for publication 27 September 2016

Published 24 October 2016



CrossMark

## Abstract

Grafting of polyethylene glycol (PEG) to ultrasmall photoluminescent silicon dots (SiDs) is expected to improve and expand the applications of these particles to aqueous environments and biological systems. Herein we report a novel one-pot synthesis of robust, highly water compatible PEG-coated SiDs (denoted as PEG-SiDs) of  $(3.3 \pm 0.5)$  nm size. The nanoparticles' synthesis is based on the liquid phase oxidation of magnesium silicide using PEG as reaction media and leading to high PEG density grafting. PEG-SiDs enhanced photophysical, photosensitising, and solution properties in aqueous environments are described and compared to those of 2 nm size PEG-coated SiDs with low PEG density grafting (denoted as PEG-NHSiDs) obtained from a multistep synthesis strategy. PEG-SiDs form highly dispersed suspensions in water showing stable photoluminescence and quantum yields of  $\Phi = 0.13 \pm 0.04$  at 370 nm excitation in air-saturated suspensions. These particles exhibited the capacity of photosensitising the formation of singlet molecular oxygen, not observed for PEG-NHSiDs. PEG robust shielding of the silicon core luminescent properties is further demonstrated in bio-imaging experiments stressing the strong interaction between PEG-SiDs and *Staphylococcus aureus* smears by observing the photoluminescence of particles. PEG-SiDs were found to be nontoxic to *S. aureus* cells at concentrations of  $100 \text{ mg ml}^{-1}$ , though a bacteriostatic effect on *S. aureus* biofilms was observed upon UV-A irradiation under conditions where light alone has no effect.

 Online supplementary data available from [stacks.iop.org/NANO/27/475704/mmedia](http://stacks.iop.org/NANO/27/475704/mmedia)

Keywords: photoluminescence, *S. aureus*, singlet oxygen, aqueous environments, silicon dots, PEGylation, one-step synthesis

(Some figures may appear in colour only in the online journal)

## Introduction

Luminescent silicon nanoparticles of 1–4 nm size (SiDs), also known as silicon quantum dots, were shown to offer the potential to significantly improve existing methods of

fluorescent labelling and cancer diagnosis and treatment, as alternative materials for organic dyes and toxic cadmium-based quantum dots [1–7]. Among the properties of interest of SiDs are their high photoluminescence (PL), good biocompatibility, tuneable surface functionalization for drug

delivery, and their capability for singlet oxygen ( $^1\text{O}_2$ ) and superoxide ( $\text{O}_2^-$ ) photosensibilization [5, 8, 9]. Surface modifications as coating/linking with substances leading to an increased solubility, biocompatibility, targeting potential, and circulation time of the particles in the biological systems is an actual need [10, 11] to increase the biological uses of SiDs. However, the PL, stability, and the yield of the generation of reactive oxygen species of SiDs strongly depend on the control of the synthesis procedures and the nature of their surface modification [8, 9, 12]. In this context, production of SiDs that are chemically and optically stable in aqueous environments and still maintain their photosensitising ability is the foremost important step for their technological uses as therapeutic agents. Besides, and not less important, therapeutic photosensitizers (PS) should be of constant composition, of simple and inexpensive synthesis procedures, non-cytotoxic in the dark but with the potential to induce cytotoxicity under irradiation.

Surface coating with nontoxic, highly water soluble, polyethylene glycol (PEG) is a current strategy in therapeutic delivery, as it is reported to lengthen the *in vivo* lifetime of diverse drugs and nanomaterials by evading macrophage-mediated uptake and removal from the systemic circulation [13, 14]. Attached PEG conformations named as ‘mushroom’ and ‘brush’ are formed at low and high PEG chain densities, respectively. Conformation is reported to affect PEG coating flexibility and hydrophilicity, and consequently aqueous solubility and the interaction with biomolecules [15]. Conformation may also affect the coating shielding of the reactive zero-dimensional silicon semiconductor core, thus determining the SiDs chemical and optical stability in aqueous suspensions. Accomplishing successful PEGylation of SiDs depends on the synthesis procedure used for obtaining the silicon core, its surface chemistry, and the method used for conjugation, as demonstrated by recent literature reports on the multistep synthesis of PEG-coated SiDs [8, 16].

Among the extended uses of PEG, several studies report an inhibition of biofilm adhesion on various PEG-coated surfaces [17–19]. In particular, *S. aureus* bacterial adhesion has been reported to persist on newly formed brushy PEGylated surfaces, but to be almost completely detached after relaxation of the brushes in buffer for 12 h [20]. Since several *S. aureus* strains are considered important human pathogens in hospital-borne infections [21] and whose principal mode of transmission is the handling of contaminated materials [22], PEG coating of SiDs may be a viable strategy to provide the particles’ resistance to *S. aureus* growth during storage and use.

Herein, we describe a novel one-pot synthesis strategy developed to obtain water-dispersible, stable, covalently bonded PEG-coated SiDs with high PEG density, denoted as PEG-SiDs. The solution and photoluminescent properties and the reactive oxygen species photosensitising ability of PEG-SiDs in aqueous suspensions were determined and compared to those of lower density PEGylated SiDs, denoted as PEG-NHSiDs, obtained by a multistep synthesis procedure. The conservation of the PL and photosensitising properties of PEG-SiDs in aqueous suspensions and biological media were

evaluated. To that purpose, experiments with *S. aureus* biofilms grown in the presence of PEG-SiDs were performed.

## Experimental

### Materials

Materials used are listed in the online supporting information under the title ‘Experimental—Materials’.

**Equipment and physicochemical assays.** Details of standard equipment used for particle characterisation, such as Fourier transformed infrared spectroscopy (FTIR), dynamic light scattering, transmission electron microscopy (TEM), PL and anisotropy experiments, singlet oxygen phosphorescence detection, and fluorescence microscopy are provided in the online supporting information under the title ‘Experimental—Equipment’.

Gel electrophoresis was performed using a 1% agarose gel in Tris-acetate-EDTA (TAE) buffer of pH 8 as a support and a TAE buffer of pH 8 as a moving phase. The electrophoresis was run for 30 min at an applied constant voltage of 100 V. The thermal behaviour of the powders in an oxygen environment was studied by thermal gravimetric analysis (TGA) using a Rigaku Serie Thermo Plus Evo instrument. The thermal programme involved an initial temperature of 30 °C followed by a 10 °C min<sup>-1</sup> ramp up to 900 °C.

The attenuation spectra were recorded with a double-beam Shimadzu UV-1800 spectrophotometer in a 1 cm quartz cuvette at a scan rate of 300 nm min<sup>-1</sup> and 1 nm bandpass. Diffuse transmittance spectra were recorded with a double-beam PGI-T90+ UV-vis spectrophotometer equipped with a BaSO<sub>4</sub> integrating sphere in a 0.1 cm quartz cuvette, and compared to the attenuation spectra obtained under the same excitation configuration to evaluate possible spectral distortions due to scattering.

To estimate the PL quantum yield ( $\Phi$ ), emission spectra were collected exciting suspensions of <0.1 absorption at 370 nm. Identical measurements (excitation conditions, lamp energy, and spectrometer band-pass) were performed with 9,10-diphenylanthracene solutions in cyclohexane, used as PL reference [23].

Singlet oxygen quantum yields,  $\Phi_{\Delta}$ , were determined from the comparison of the signal intensity of the 1270 nm phosphorescence traces generated by the particles suspensions upon excitation with different laser fluence and those of the reference TPP under similar solution absorbance at 355 nm and experimental setup [24].

Steady-state  $^1\text{O}_2$  generation experiments involved the irradiation of air-saturated aqueous suspensions of the particles contained in a closed vessel with a Southern New England Ultraviolet Co RMR-3500 lamp. The probe SOSG was used to specifically detect  $^1\text{O}_2$  formation. To that purpose, 1.45 ml aliquots of PEG-functionalized SiDs aqueous suspensions of 0.46 absorbance at 350 nm were irradiated in the presence of 0.63 mg l<sup>-1</sup> of SOSG. The

SOSG- $^1\text{O}_2$  adduct formed was detected by its fluorescence with maximum emission at 525 nm upon 504 nm excitation. To quantify  $^1\text{O}_2$  in these experiments, the 525 nm emission was calibrated against the SOSG- $^1\text{O}_2$  fluorescence produced by known amounts of  $^1\text{O}_2$  generated by aqueous suspensions of methylene blue, MB, under similar experimental conditions ( $\Phi_{\Delta} = 0.55$ ) [25]. The lamp photon flux was measured with the potassium ferrioxalate chemical actinometer [26].

Superoxide concentrations were measured indirectly by an enzymatic colorimetric method employing a commercial kit for cholesterol quantification, Colestat Wiener Lab Argentina, determining  $[\text{H}_2\text{O}_2]$ . Calibration curves were performed using standard  $\text{H}_2\text{O}_2$  commercial solutions.

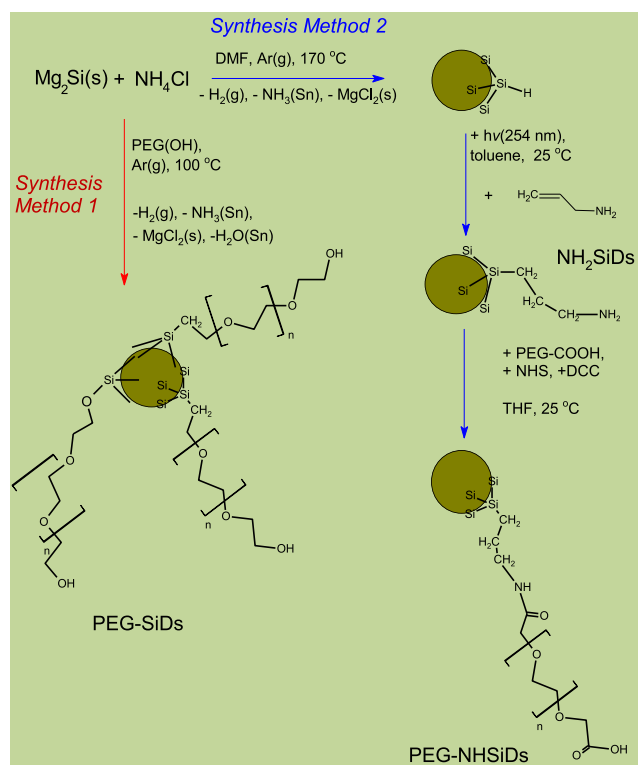
**Bilinear regression analysis.** For low chromophore absorbance, the bilinear regression analysis takes advantage of the linearity of the steady-state PL emission intensity at the given emission wavelength,  $I(\lambda_{\text{em}})$ , with both, the absorption coefficient of the fluorophore,  $\varepsilon(\lambda_{\text{exc}})$ , and the factor  $F(\lambda_{\text{em}})$  reflecting the shape of the emission spectrum. The analysis retrieves information from the experimental excitation-emission matrix on the minimum number of species and on their relative emission and absorption spectra [27].

**Biological standard procedures.** Agar diffusion assay [28], biofilm formation protocol [29], and bacterial counting are described in the online supporting information under the title ‘Biological Standard Procedures’.

**Bacterial cultures.** *S. aureus*. ATCC 25923 were inoculated in 100 ml of nutrient broth (NB) and grown overnight at 31 °C with shaking (250 rpm). The cultured *S. aureus* was further diluted with fresh NB in a glass flask to an optical density at 590 nm  $\text{OD}^{590} = 0.5$  (ca.  $1 \times 10^9$  bacteria  $\text{ml}^{-1}$ ). This bacterial suspension was used for the biological assays.

**Photodynamic antimicrobial assays.** Planktonic bacteria were grown ( $\text{OD}^{590} = 0.5$ ) and 1 ml of an aqueous suspension of PEG-SiDs of 2.6 absorbance at 355 nm was added to the bacterial culture and incubated for biofilm formation. Biofilmed glasses were thoroughly washed before irradiation. The irradiation system consisted of a black box enclosing a 6 cm diameter petri dish containing 10 ml of 1:10 diluted NB in PBS supporting the  $0.25 \text{ cm}^2$  glasses with the biofilms. The dish was placed at 10 cm from a Southern New England Ultraviolet Co RMR-3500 lamp emitting light of 350 nm. The photon flux reaching the glass slides was  $3.5 \times 10^{-11}$  Einstein  $\text{s}^{-1} \text{ cm}^{-2}$ , as determined by ferrioxalate actinometry. Bacteria were counted before and after irradiation, following the protocol already described. Biofilms formed in the absence of SiDs were used as controls. Experiments were performed in quadruplicate.

All biological experiments were statistically analysed with the aid of the one way ANOVA test and Tukey HSD post-hoc test.



**Scheme 1.** Synthesis pathways followed to obtain  $\text{NH}_2\text{SiDs}$ , PEG-NHSiDs and PEG-SiDs. The green spheres represent 1.3–1.7 nm size SiDs core comprised of ca. 40 surface Si atoms [32].

## Results and discussion

### Synthesis and characterisation of PEG-coated silicon dots

Two methods were employed to obtain PEG-coated SiDs. The experimental details of the synthesis are described in the online supporting information under the title ‘Synthesis Procedures’. Synthesis method 1 involves a novel one-pot synthesis in which magnesium silicide in PEG as reaction media was oxidised to PEG-terminated SiDs, denoted as PEG-SiDs. Synthesis method 2 consists of a multi-step procedure, starting with the oxidation of magnesium silicide to H-terminated SiDs [30], further surface functionalization of these particles with propylamine [8] to yield  $\text{NH}_2\text{SiDs}$ , and linking of the latter to carboxyl-terminated PEG through an amide bond to obtain PEG-NHSiDs. Scheme 1 shows a flow diagram of the particle synthesis. Both methods involve the heterogeneous oxidation reaction of  $\text{Mg}_2\text{Si}$  with  $\text{NH}_4\text{Cl}$  at temperatures of 100 °C–170 °C to obtain the SiDs core. While oxidation of  $\text{Mg}_2\text{Si}$  in organic solvents yields H-terminated SiDs [31], the use of PEG as solvent in method 1 favours the formation of stable Si–C and Si–O–C bonds with PEG chains instead of reactive surface Si–H bonds, as will be discussed later on.

The FTIR spectra of the different particles shown in figure 1 and analysed in the online supporting information under the title ‘FTIR Data’ confirm the surface derivatization of the SiDs obtained from the different strategies. From this analysis it is important to recall that the small peaks appearing

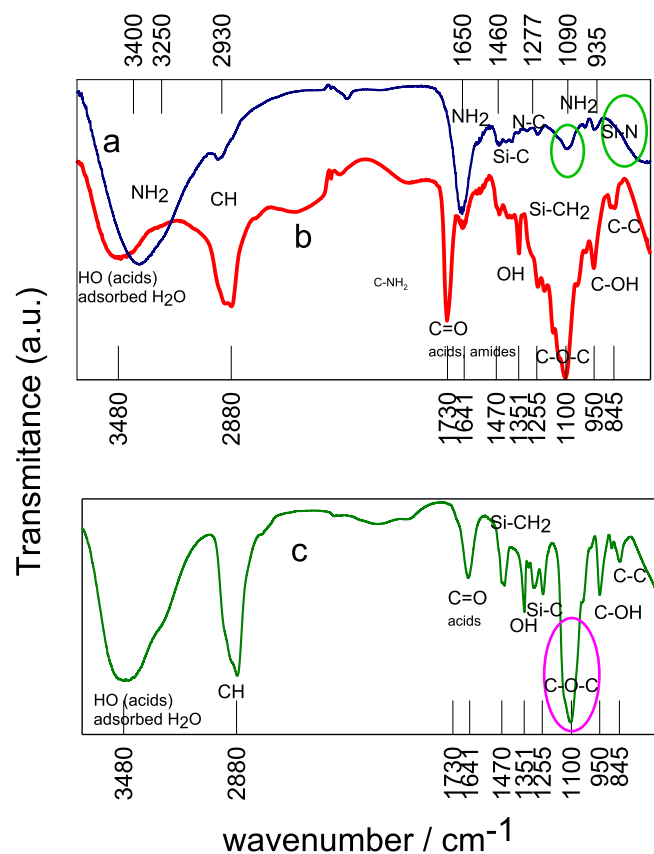


**Figure 1.** FTIR spectra of  $\text{NH}_2\text{SiDs}$  (top, blue spectrum a), PEG-NHSiDs (red, medium spectrum b), and PEG-SiDs (green, bottom spectrum c). Circles denote the peaks discussed in the text.

at 1250 and 1450  $\text{cm}^{-1}$  observed for PEG-SiDs assigned to Si-C and Si-CH<sub>2</sub> vibrations, strongly support the attachment of PEG chains to SiDs through Si-C bonds. However, PEG attachment through Si-O-C bonds cannot be unambiguously determined as characteristic signals due to Si-O-C vibrations also appear around 1100  $\text{cm}^{-1}$  in the same region than C-O-C stretch of PEG polyether chain [33].

On the other hand, the absence of a band at 880  $\text{cm}^{-1}$  attributed to Si-N vibrations in the IR spectrum of  $\text{NH}_2\text{SiDs}$  indicates that N-bonding to Si in secondary products of the radical mechanism involved in the synthesis reaction [9], are not formed. Moreover, any oxidation of the  $\text{NH}_2\text{SiDs}$  surface is expected to be of little significance as any contribution of Si-O-Si bond vibrations to the 1090  $\text{cm}^{-1}$  peak is discarded based on the fact that the C-N stretch (1090  $\text{cm}^{-1}$ ) to  $\text{NH}_2$  scissoring (1600  $\text{cm}^{-1}$ ) peak area observed here is on the order expected for aliphatic primary amines. Finally, the presence of a small peak at 1640  $\text{cm}^{-1}$  in PEG-NHSiDs assigned to  $\text{NH}_2$  in primary amines indicates the presence of PEG-free propylamine groups.

Gel electrophoresis experiments using 1% agarose gels in TAE buffer of pH 8 showed different running directions for  $\text{NH}_2\text{SiDs}$  and PEG-NHSiDs (see figure 2 in online supporting information), as expected for the change in the surface charge supported by  $\text{NH}_3^+$  groups in  $\text{NH}_2\text{SiDs}$  and  $\text{COO}^-$  in PEG-NHSiDs, thus confirming the functionalization of  $\text{NH}_2\text{SiDs}$

with carboxyl-terminated PEG chains. On the other hand, PEG-SiDs almost remained in the seeding channel as expected from the particle efficient coverage with HO-terminated PEG chains, in line with the reported decrease in Z-potential with increasing PEG coverage of silica surfaces [14].

TEM micrographs of  $\text{NH}_2\text{SiDs}$  and PEG-SiDs are depicted in figures 2(A) and (B), respectively. Corresponding Feret diameter ( $D_F$ ) distribution histograms are shown in the inset of the figures. From the histogram shown in figure 2(A), an average  $D_F = (1.8 \pm 0.4)$  nm is obtained for  $\text{NH}_2\text{SiDs}$ . The size histogram of 420 well-dispersed PEG-SiDs depicted in figure 2(B) inset allows a Lognormal-type distribution fitting yielding an average  $D_F = (3.3 \pm 0.5)$  nm. Since HRTEM images (not shown) of  $\text{NH}_2\text{SiDs}$  and PEG-SiDs showed no evidence of crystalline structures, these particles are assumed to be amorphous.

**Photoluminescence experiments.** The PL emission spectrum of aqueous suspensions of  $\text{NH}_2\text{SiDs}$ , PEG-NHSiDs, and PEG-SiDs show a clear dependence with the excitation wavelength. Such dependence strongly suggests the contribution to the overall luminescence of particles of different size and surface morphology and composition. Particle suspensions used for PL analysis were of <0.075 absorbance at 300 nm. Under such conditions, dilution of the suspensions retrieved the same emission spectrum and the area under the emission spectrum linearly decreases with the dilution factor, as depicted in the supporting information under the title ‘Photoluminescence’. Therefore, any contribution to the observed PL due to particle agglomeration may be discarded under the experimental conditions used [34].

The contribution of different emitters to the overall PL excitation-emission matrix, EEM, was analysed on the assumption that the SiDs suspension comprises distinct, individual chromophores, exhibiting excitation wavelength-invariant PL emission spectra. A minimum of two well differentiated family of contributing emitters to the overall PL is predicted from the bilinear analysis of the PL EEM of aqueous suspensions of each SiDs sample. Namely, *a'* and *b'* represent the contributing emitters to the PL-EEM of  $\text{NH}_2\text{SiDs}$ , *a''* and *b''* those of PEG-NHSiDs, and *a'''* and *b'''* those of PEG-SiDs, all shown in figure 3. However, it should be recalled that the contribution of highly superposing species to emitters ‘*a*’ and ‘*b*’ cannot be neglected.

Within the error of the determination, the excitation and emission spectra of contributing species *b'*, *b''*, and *b'''* are similar thus suggesting that the PL of these contributing chromophores might involve comparable transitions. A similar observation holds for species *a'*, *a''*, and *a'''* (see superposing normalised spectra for species ‘*a*’ and ‘*b*’ in figure 4 of the online supporting information). The mean energy gap (EG) of charge carriers was evaluated for each individual contributing species using the PL excitation spectrum threshold, see table 1. EG values of ca. 2.5–2.6 eV were observed for species *a'*, *a''*, and *a'''* while

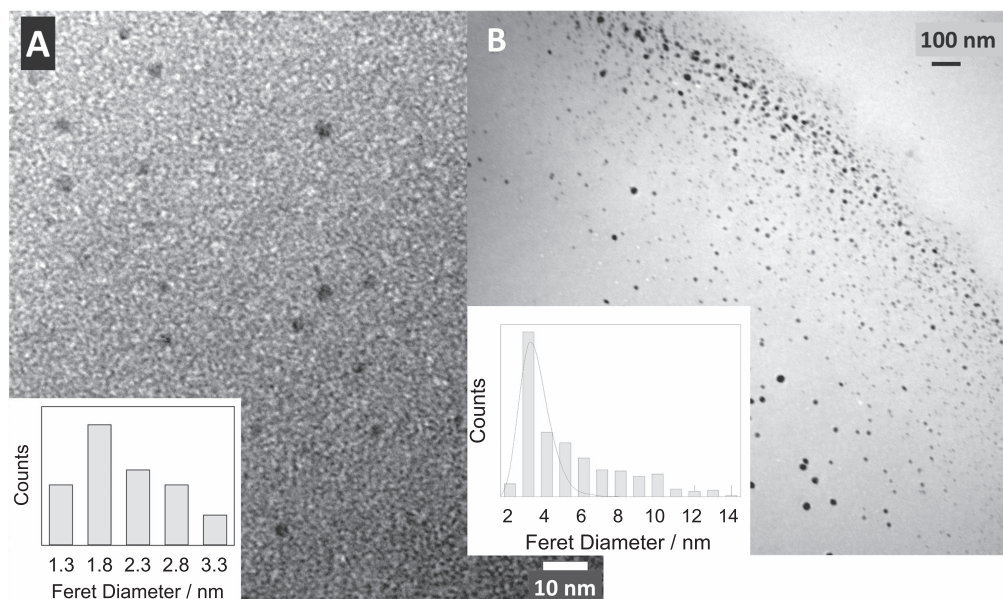


**Figure 2.** TEM image of (A)  $\text{NH}_2\text{SiDs}$  and (B) PEG-SiDs. Inset A: size histogram of 105 well-dispersed  $\text{NH}_2\text{SiDs}$ . Inset B: associated size histogram of 420 well-dispersed PEG-SiDs and fitting to a lognormal distribution (solid line).

values of ca. 3.0 eV were observed for species  $b'$ ,  $b''$ , and  $b'''$ . Despite the similar transitions involved, PEG-SiDs and PEG-NHSiDs luminescence quantum yields in air-saturated aqueous suspensions,  $\Phi = 0.13 \pm 0.04$  and  $0.010 \pm 0.005$ , respectively, are extremely different.

On the other hand, time-resolved PL anisotropy experiments (see online supporting information—anisotropy) yield complementary information of the overall size of the SiDs core and its surface coating, since size estimation relies on the rotational correlation time of the particles. PL anisotropy measurements were performed at 298 K by detecting selectively species  $a'$ ,  $a''$ , and  $a'''$  (388 nm excitation and 450 nm PL detection). Each PL anisotropy decay could be well fitted to a single exponential function,  $r(t) = r_0 \times \exp(t/\theta)$ , which confirms the spherical shape of the emitting SiDs core. The values for the intrinsic anisotropy ( $r_0$ ) and the rotational correlation time ( $\theta$ ) obtained as best-fit parameters are shown in table 1. All the particles show, within the experimental error,  $r_0 \approx 0.4$  thus indicating that  $a'$ ,  $a''$ , and  $a'''$  show parallel absorption and emission transition moments, and further supports that coating with either PEG or propylamine does not affect the overall density of states within the capture volume of spatially confined carriers leading to PL in amorphous SiDs [35].

Using the value 0.0091 poise for the shear viscosity of water at 25 °C and the observed  $\theta$  values, the mean hydrodynamic sizes ( $D_{\text{hyd}}$ ) of species  $a'$ ,  $a''$ , and  $a'''$  were determined from the Stokes equation and shown in table 1.  $\text{NH}_2\text{SiDs}$  and PEG-SiDs sizes obtained from anisotropy data are in line with those determined from TEM images, see table 1.  $D_{\text{hyd}}$  values of 1.9(4) and 2.2(5) nm obtained for  $\text{NH}_2\text{SiDs}$  and PEG-NHSiDs indicate that PEG multistep derivatization does not significantly contribute to the hydrodynamic size.

SiDs of different synthesis procedures and of ca. 1.8–1.9 nm size, are reported to show emission maxima around 450 nm [6] and EG values of 2.5 eV [36–38]. The PL properties and size of species  $a'$  being in coincidence with literature reports for 1.8 nm size SiDs, may be regarded at a first glance, as of quantum confinement origin. However, as already discussed, the similar PL properties and  $r_0$  values of species  $b'''$  and  $b'$  strongly indicate a comparable nature of the emissive sites for both emitters. Such analysis is difficult to sustain for a recombination of excitons due to the presence of alkyl-terminated silicon atoms (Si–O–R) on the surface of PEG-SiDs. In fact, Si–OR groups are expected to introduce surface states able to participate in the overall PL [6, 9, 39–41] with reported PL red shifts of ca. 0.4 eV compared to alkyl-terminated SiDs of the same size distribution [41]. A most important experimental condition not yet taken into account in the present discussion is the fact that water is the solvent used in these experiments. Literature reports are irrefutable in indicating that the optical properties of silicon quantum dots are strongly influenced by circumjacent surface-adsorbed water molecules [5, 6, 39, 42]. Recently reported density functional calculations investigating the effect of water on Si quantum dots [42] indicate that in humid environments PL is dominated by the stretching of Si–Si bonds, which could be explained by a self-trapped exciton model. The similar transitions observed here for PEG-NHSiDs and PEG-SiDs could be easily understood if a self-trapped model is responsible for the observed PL.

Yet more striking is the coincidence between the PL excitation and emission spectra of species  $a'$  with those of 3 nm size silicon dots with  $\text{Si-SiO}_x(-\text{OC}_3\text{H}_7\text{CO}_2\text{CH}_3)$  terminations in aqueous suspensions [5]. It should be recalled that no Si–SiO<sub>x</sub> structures were observed for  $\text{NH}_2\text{SiDs}$  before being suspended in an aqueous environment, though partial oxidation of constrained surface Si–Si bonds to more

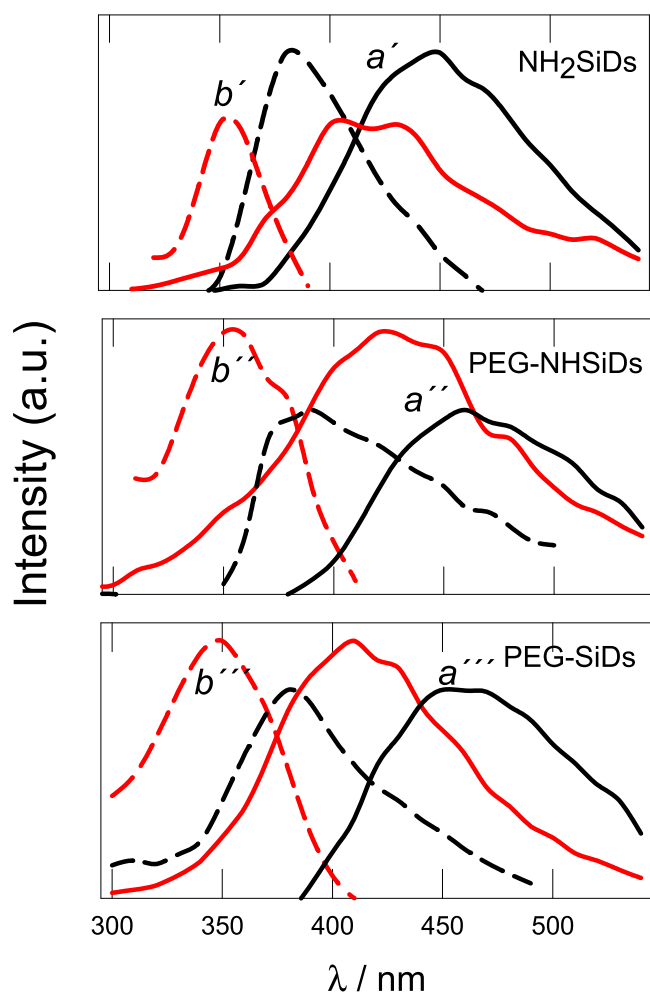


**Figure 3.** PL emission (solid lines) and PL excitation (dashed lines) spectra at 298 K of aqueous suspensions of the two contributing emitters (identified by the red and black curves) obtained from the bilinear analysis of the PL-EEM of  $\text{NH}_2\text{SiDs}$  ( $a'$  and  $b'$ ), PEG-NHSiDs ( $a''$  and  $b''$ ), and PEG-SiDs ( $a'''$  and  $b'''$ ).

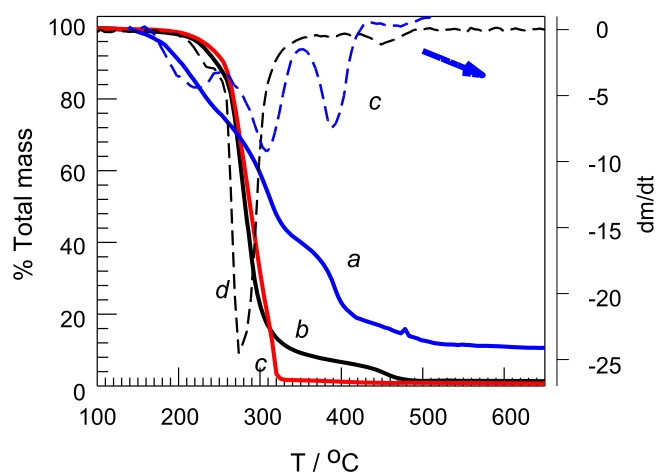


**Figure 4** TGA of (a) PEG-NHSiDs, (b) PEG-SiDs, and (c) PEG, performed in oxygen atmosphere. Dotted lines (c) and (d) stand for PEG-NHSiDs and PEG-SiDs derivative curves, respectively.

chemically stabilised Si–O–Si and Si–O–H bonds in the presence of water cannot be discarded [43].

From the previous discussion it becomes clear that the PL origin of species ‘a’ and ‘b’ cannot be determined from the present experiments since water as a solvent has an important role which still needs being elucidated. To unambiguously understand the effect of water on the particles photophysics and morphology, a systematic survey on the effect of the solvent, size, and nature of the surface functional groups on the particles PL and morphology is needed, which is out of the scope of the present study.

*Estimation of PEG content from TGA measurements.* TGA measurements of PEG-NHSiDs and PEG-SiDs in  $\text{O}_2$  atmosphere were obtained to determine the PEG content of the particles. The corresponding TGA curve for PEG-SiDs, see figure 3, shows an important weight loss of ca. 90.5% between 100 °C and 350 °C, which may be assigned to the loss of surface-attached PEG chains, in line with the TGA curve of PEG, also shown in figure 4, and with the reported behaviour of surface unbound and bound PEG [44, 45]. Silicon loss might take place at  $T > 350$  °C, as also reported for poly(vinylpyrrolidone)-capped SiDs [46]. Moreover, literature reports on bare SiDs indicate that oxidation of Si powder in air is not significant below 600 °C [47]. Therefore, the 9% weight remaining at  $T > 350$  °C may be assigned to the silicon content in the core.

As already discussed, estimates of PEG-SiDs silicon core sizes from PL experiments are of the order of 1.8 nm. Theoretical calculations [34] for this particle size predict ca. 185 Si atoms, of which 76 surface atoms may be derivatized [8]. A rough estimate taking the average molecular weight of PEG and that calculated for a 1.8 nm size Si core (5195), yields ca. 78 PEG chains attached to each core size considering the TGA losses. Thus, all surface silicon atoms are bonded to PEG chains, in line with a high PEG density coating. A rough estimation of the PEG shell thickness of 0.8 nm is obtained from the difference in  $D_{\text{hyd}}$  values depicted in table 1 for  $\text{NH}_2\text{SiDs}$  and PEG-SiDs. Considering that water is a good solvent for PEG chains, the end-to-end length of free  $\text{PEG}_{600}$  in aqueous solution reported in the literature [48–50],  $\langle h^2 \rangle^{1/2} \approx 1.5$  nm may be an upper estimation of the average PEG-shell thickness in a brush-type configuration. Therefore, PEG conformation in PEG-SiDs may be assumed more like a brush-type than a ‘mushroom’ conformation.

On the other hand, PEG-NHSiDs show a more complex TGA pattern observing almost overlapped elimination of the propyl amine coating and grafted PEG. However, following the previous discussion, the mass loss of ca. 60% at  $T < 350$  °C may be assigned to the elimination of the attached PEG and propylamine moieties. The remaining 40% mass at  $T < 350$  °C might be assigned to the silicon core. Taking the average molecular weight of 5195  $\mu$  for a 1.8 nm size Si core, *vide supra*, an average number of propylamine-attached PEG chains per PEG-NHSiDs in the range between 5 and 11 are estimated on the assumption that all surface Si

**Table 1.** Energy gap (EG), maximum PL emission ( $\lambda_{em}^{max}$ ), intrinsic anisotropy ( $r_0$ ), rotational correlation time ( $\theta$ ), and hydrodynamic diameter ( $D_{hyd}$ ) of the contributing species to the overall emission of  $NH_2SiDs$ , PEG-NHSiDs, and PEG-SiDs aqueous suspensions at 298 K. ND stands for 'not determined'.  $D_F$  stands for the Feret diameter determined from TEM images. Numbers in brackets stand for the error in the last digit.

Particle	Species	EG (eV)	$\lambda_{em}^{max}$ (eV)	$r_0$	$\theta$ (ns)	$D_{hyd}$ (nm)	$D_F$ (nm)
$NH_2SiDs$	$a'$	2.45(5)	2.53–2.43	0.38(5)	1.0(2)	1.9(4)	1.8(4)
	$b'$	2.95(5)	2.9(5)	ND	ND	ND	
PEG-NHSiDs	$a''$	2.50(5)	2.75–2.58	0.35(5)	1.1(2)	2.2(5)	ND
	$b''$	3.01(5)	2.91(5)	ND	ND	ND	
PEG-SiDs	$a'''$	2.48(5)	2.75–2.58	0.39(5)	1.8(3)	3.6(7)	3.3(5)
	$b'''$	3.06(5)	3.02(5)	ND	ND	ND	

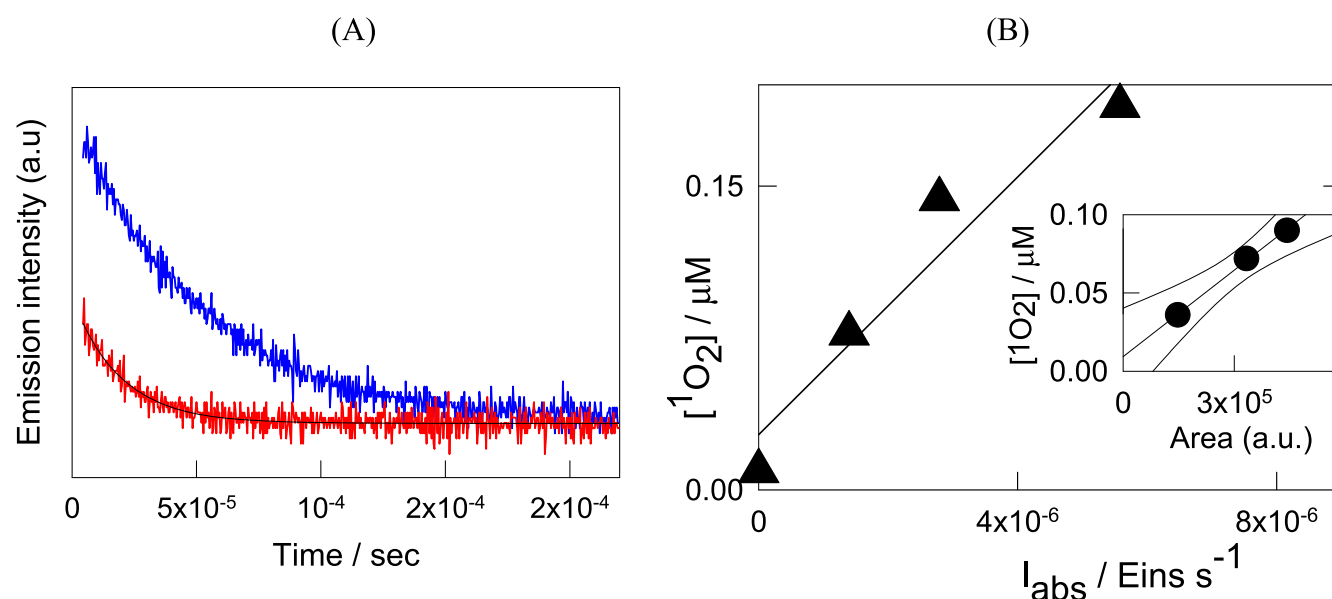


**Figure 5.** (A)  $^1O_2$  NIR phosphorescence traces at 1270 nm obtained upon 355 nm excitation of TPP (upper curve) and PEG-SiDs (lower curve) suspensions in air-saturated acetonitrile solution. Black lines stand for the curve fitting to a single exponential decay. (B) Plot of  $[^1O_2]$  generated during 350 nm irradiation of different (PEG-SiDs) in aqueous suspensions versus the absorption intensity of the suspensions at 350 nm. Inset:  $[^1O_2]$  produced by a singlet oxygen reference against SOSG- $^1O_2$  fluorescence (see text).

atoms are covered with propylamine groups and only those attached to the PEG chains, respectively. Therefore, between 5% and 15% of the surface silicon atoms are functionalized, thus supporting a low PEG density coating in line with a PEG shell thickness  $\leq 0.3$  nm, as estimated from the difference in  $D_{hyd}$  values depicted in table 1 for  $NH_2SiDs$  and PEG-NHSiDs.

PEG-SiDs having a luminescence ten times higher than that of PEG-NHSiDs may be attributed to the shielding effect exerted by the thick PEG shell on PEG-SiDs silicon core. PEG-shielding of the silicon core provides PEG-SiDs of stable PL under a number of situations of importance for the technological uses of the particles in biological systems, such as: three months storage in air-saturated aqueous suspensions in the dark at room temperature, resuspension after freezing, and sterilisation at 121 °C and 2 atm during 20 min. Moreover, PEG-SiDs irradiation with light of 350 nm and  $3.3 \times 10^{-11}$  Einstein  $cm^{-3} s^{-1}$  absorbed photon flux, bleaches the PL of 1 mg  $ml^{-1}$  particles by 1.5% and by

10% after 2 and 4 h irradiation, respectively, thus supporting a photostable particle structure in aqueous suspensions.

**Singlet oxygen generation.** The singlet oxygen,  $^1O_2$ , photosensitising capacity of the particles in organic solvent suspensions was evaluated using the characteristic  $^1O_2$  NIR phosphorescence at 1270 nm via time-resolved laser techniques already described. Mainly PEG-SiDs showed the generation of traces at 1270 nm upon 355 nm irradiation, as shown in figure 5. A quantum yield of  $^1O_2$  generation  $\Phi_{\Delta} = 0.12 \pm 0.04$  was obtained in acetonitrile considering  $\Phi_{\Delta R} = 0.6$  for the reference TPP in the same solvent [24]. The obtained value is of the order reported for SiDs of different synthesis procedures and suspended in organic solvents [5]. From the fitting to an exponential decay of the traces in figure 4,  $^1O_2$  lifetimes ( $\tau_{\Delta}$ ) were determined to be  $43 \pm 7$  and  $19 \pm 1 \mu s$  for the reference and PEG-SiDs in acetonitrile, respectively. While values of  $39 \pm 10 \mu s$  are on the order expected for  $^1O_2$  lifetime in acetonitrile [25], the

smaller value observed for PEG-SiDs might suggest a reaction between  $^1\text{O}_2$  and the particles surface. In fact, PEG terminal hydroxyl groups are expected to be reactive towards  $^1\text{O}_2$  [51].

Formation of singlet oxygen in aqueous suspensions was further confirmed with the probe Singlet Oxygen Sensor Green, SOSG. After continuous irradiation with light of 350 nm, aqueous suspensions of PEG-SiDs in the presence of SOSG show green fluorescence due to the formation of SOSG- $^1\text{O}_2$  adduct [52, 53]. The fluorescence of the adduct was calibrated ( $r^2 = 0.998$ ) against [ $^1\text{O}_2$ ] produced upon 350 nm irradiation of an aqueous solution of MB of 0.01 absorbance (1 cm optical path length) at 350 nm, on the assumption that all  $^1\text{O}_2$  produced reacts with SOSG, see figure 5(B) inset. Therefore, from the slope of the plot of [ $^1\text{O}_2$ ] versus the absorbed light intensity ( $I_{\text{abs}}$ ) of PEG-SiDs aqueous suspensions of different concentrations, see figure 5(B), a lower limit  $\Phi_{\Delta} = 0.03 \pm 0.01$  is obtained, of the order reported for SiDs of different origin in aqueous suspensions [5]. In line with the observed water quenching of the luminescence quantum yields [9], lower  $\Phi_{\Delta}$  values are observed in aqueous suspensions than in organic solvents. Thus, compared to organic solvents, water plays a major role in non-radiative deactivation channels of the photoactive excited state.

Organic suspensions of  $\text{NH}_2\text{SiDs}$  and PEG-NHSiDs showed no emission traces at 1270 nm upon excitation with light of 355 nm. These results are in line with previously reported studies involving SiDs obtained from a different synthesis procedure but with identical surface groups [8]. An enhanced quenching efficiency by propylamine groups grafted to SiDs was suggested to be the cause of the severe diminution in the  $^1\text{O}_2$  photosensitising capacity of the particles.

Formation of superoxide radical anion,  $\text{O}_2^{\cdot-}$ , upon 350 nm irradiation of aqueous suspensions of PEG-SiDs and PEG-NHSiDs was investigated employing an indirect commercial enzymatic colorimetric method measuring [ $\text{H}_2\text{O}_2$ ]. Since, within the sensibility of the method, no traces of formed  $\text{H}_2\text{O}_2$  was observed for both particle suspensions, it was assumed that [ $\text{O}_2^{\cdot-}$ ]  $\ll 1 \times 10^{-5}$  M.

**Toxicity evaluation of  $\text{NH}_2\text{SiDs}$ , PEG-NHSiDs, and PEG-SiDs.** The toxicity of  $\text{NH}_2\text{SiDs}$ , PEG-NHSiDs, and PEG-SiDs in aqueous suspensions against bacteria was evaluated. A diffusion method based on the aura inhibition on sense discs soaked with the particles which is placed on the surface of the Muller Hinton agar medium inoculated with *S. aureus* was used following the protocol described in the online supplementary information. None of the particles exhibited a significant inhibition zone indicating that the particles showed no toxicity towards *S. aureus* under concentrations of  $100 \text{ mg ml}^{-1}$ .

**Bacterial growth in the presence of PEG-SiDs.** Considering that PEG-SiDs showed lower aggregation tendency in aqueous suspensions than PEG-NHSiDs and the capacity for  $^1\text{O}_2$  formation (not observed for PEG-NHSiDs), they are

suitable for biological studies and were selected to test the interaction with bacteria in biofilms. Thus, biofilms were grown on normal glass substrates in a growth medium containing PEG-SiDs in suspension, as described in the experimental section. After 2 h incubation, the obtained biofilms were thoroughly washed to eliminate loosely adherent particles.

Biofilms were observed by fluorescence microscopy using HQ365/30 and HQ430/30 excitation and emission filters, respectively, to detect the luminescence of PEG-SiDs and to avoid cells autofluorescence. In these experiments, staining dyes were not used to avoid interferences. Corresponding images depicted in figure 6(A) clearly show that the micrometric colonies formed may be easily distinguished in experiments performed in the presence of PEG-SiDs while colonies formed in control experiments in the absence of particles remain dark. Thus, PEG-SiDs intense interaction with *S. aureus* cells is strongly suggested. Taking into account that the particles were not peeled off upon a thorough sample washing and that bacterial counting showed no statistical differences between colonies grown in the presence and absence of PEG-SiDs, see figure 6(B), a potential use of these particles for the detection of sessile *S. aureus* is suggested.

#### *Photodynamic activity of PEG-SiDs interacting with biofilms.*

To investigate the potential photodynamic antimicrobial activity of the particles, *S. aureus* biofilms grown in the presence of around 0.2–0.4  $\mu\text{mole}$  of PEG-SiDs, *vide supra*, were irradiated with light of 350 nm and  $8.7 \times 10^{-12}$  Einstein  $\text{s}^{-1}$  incident photon flux, as described in the experimental section. Corresponding blank experiments involve biofilms grown in the absence of attached PEG-SiDs. Figure 7 shows that 2 h irradiation does not affect, within the experimental error, the number of bacteria in biofilms grown in the absence of particles. However, irradiation under identical conditions reduces the number of bacteria in biofilms grown in the presence of PEG-SiDs to ca. 55%; thus indicating that PEG-SiDs show potential capacity as photosensitizer for the photodynamic reduction of viable attached bacteria.

Since the participation of  $\text{O}_2^{\cdot-}$  may be discarded due to its negligible formation, a rough estimation considering the experimental set-up used for the photodynamic antimicrobial assays, *vide supra*, and assuming that the incident photo flux is completely absorbed by the attached PEG-SiDs, indicates that a delivered  $^1\text{O}_2$  dose of  $<0.06 \mu\text{g}$  was capable of reducing about 45% of *S. aureus* cells on the biofilm grown on the  $0.25 \text{ cm}^{-2}$  glass support. Thus a bacteriostatic effect of  $^1\text{O}_2$  towards sessile *S. aureus* cells is suggested. The observed results are in line with reported studies sustaining that photodynamic therapy has the potential to rapidly reduce *S. aureus* load in infected burns, though the authors also report a fast recovery of bacterial activity following photodynamic inactivation [54]. The optimisation of the experimental variables (increasing photon irradiance, irradiation times and particle concentration) is in progress to determine a minimum inhibitory concentration for comparison with other molecular

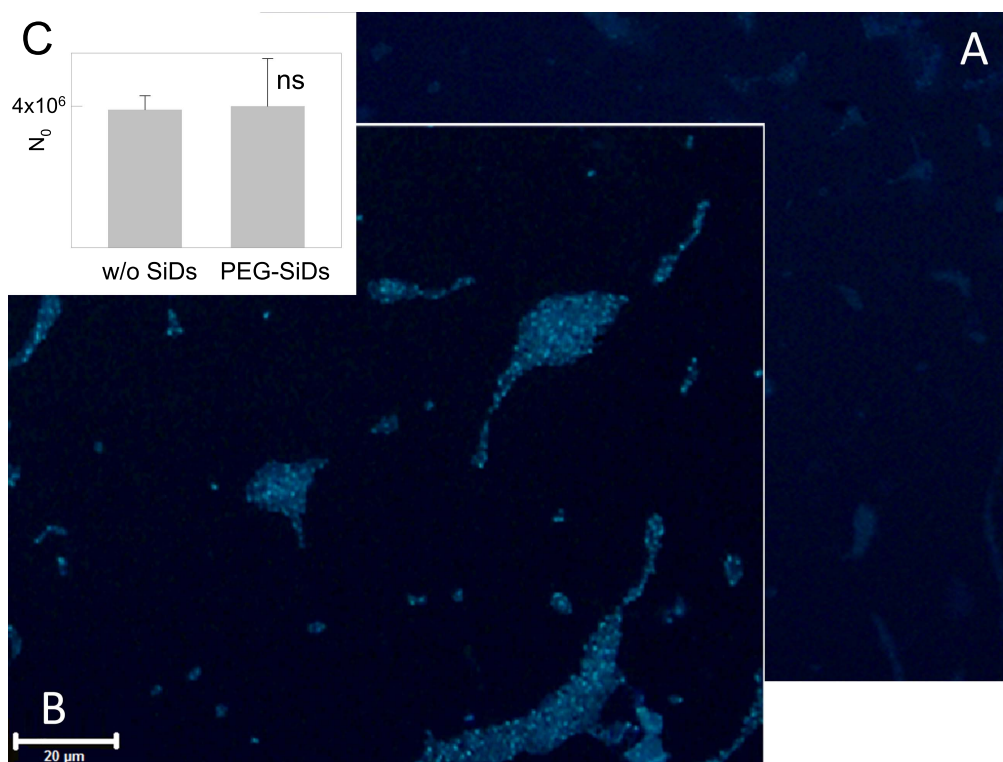


**Figure 6.** Fluorescence microscopy images ( $100\times$ ) of the smears incubated (A) in the presence and (B) absence of PEG-SiDs. Bars stand for  $20\ \mu\text{m}$  size scale. (C) Bar plot showing the number of bacteria ( $N_0$ ) in biofilms grown in the presence (PEG-SiDs) and absence (w/o SiDs) of PEG-SiDs. Error bars represent standard errors of the mean. ‘ns’ indicates no statistically significant differences. Each data is the average of four replicates.

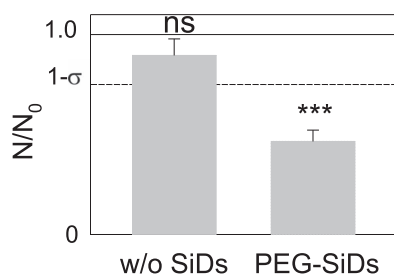


**Figure 7.** Ratio of the number of bacteria after 2 h irradiation with light of 350 nm to that in the biofilms treated in the same way but without irradiation ( $N/N_0$ ) for both, films grown in the absence (w/o SiDs) and presence (PEG-SiDs) of PEG-SiDs. Dark controls are also depicted. Error bars represent standard errors of the mean. Statistically significant differences are indicated by \*\*\*  $p < 0.001$ , ns no significant. Each bar is the average of four replicates.

PS. However, an advantage of the use of PEG-SiNPs when compared to molecular PS is its high photostability in aqueous suspensions showing low photobleaching effects.

## Conclusions

In conclusion, we synthesised highly water-dispersible, high density PEG-functionalized, blue emitting, 3 nm size bio-compatible SiDs via a facile synthesis strategy which involved the wet oxidation of  $\text{Mg}_2\text{Si}$  and the attachment of PEG in a one-pot procedure. The particles, denoted as PEG-

SiDs were compared to those obtained from a multistep strategy (denoted as PEG-NHSiDs) involving the wet oxidation of  $\text{Mg}_2\text{Si}$  synthesis of H-terminated SiDs, further coating by silylation with 2-propenylamine, and subsequent carboxyl-terminated PEG attachment through amide bonds. PEG-SiDs showed particular properties which were not observed for PEG-NHSiDs, as a high PEG density coverage compatible with a brush type conformation and the capacity for singlet oxygen photosensitisation with quantum yield  $\Phi_\Delta \geq 0.03$  in air-saturated aqueous suspensions. Moreover, PEG-SiDs suspended in air saturated aqueous solutions are stable for months, show no tendency to agglomerate, and present a PL quantum yield  $\Phi = 0.13$  upon 370 nm excitation which is higher than those of other reported water-compatible SiDs. In summary, the present results strongly indicate that surface modification with high density PEG coatings is an excellent strategy for SiDs uses in aqueous environments as it avoids water quenching of the particles luminescence, preserves the particles singlet oxygen photosensitising capacity, improves their stability, and prevents them from aggregating. Therefore, the thus obtained PEG-SiDs enhanced properties fulfil the foremost important requirements for SiDs technological uses in biology: they are of facile synthesis, are chemically and optically stable in aqueous environments, and still maintain their photosensitising ability.

Biological experiments with *S. aureus* biofilms revealed a strong bacteria/nanoparticle interaction which enabled bacteria microscopic observation by PEG-SiDs PL. PEG-

SiDs showed no toxicity towards *S. aureus* cells in the dark under concentrations of  $100 \text{ mg ml}^{-1}$ , but a bacteriostatic effect was observed under UV-A light irradiation. These observations opened new promising technological uses of the particles that worth further investigation: their use as stable fluorophores for microscopic observation of bacteria films and as PS of bacterial biofilm inhibition. Moreover, PEG-SiDs might be finely tuned upon further derivatization with active molecules as labels to obtain a new generation of target-directed bacterial sensors and PS.

## Acknowledgments

DRS, JJR and CRL thank Consejo Nacional de Investigaciones Científicas y Técnicas (CONICET, Argentina) for graduate studentships. MCG, MLD, AM and MFLM are research members of CONICET, Argentina. R Gorojod and M L Kotler (UBA) are specially thanked for their help with the Gel Electrophoresis experiments. This research was supported by grant PIP 112-200801-00356 from CONICET, I163 from UNLP and PICT 2012-1795 from ANPCyT.

## References

- [1] Burda C, Chen X, Narayanan R and El-Sayed M A 2005 Chemistry and properties of nanocrystals of different shapes *Chem. Rev.* **105** 1025–102
- [2] Gara P M D *et al* 2012 ROS enhancement by silicon nanoparticles in x-ray irradiated aqueous suspensions and in glioma C6 cells *J. Nanopart. Res.* **14** 741
- [3] Michalet X *et al* 2005 Quantum dots for live cells, *in vivo* imaging, and diagnostics *Science* **307** 538–44
- [4] Praetorius N P and Mandal T K 2007 Engineered nanoparticles in cancer therapy *Recent Pat. Drug. Deliv. Formulation* **1** 37–51
- [5] Llansola Portolés M J *et al* 2010 Silicon nanoparticle photophysics and singlet oxygen generation *Langmuir* **26** 10953–60
- [6] Cheng X, Lowe S B, Reece P J and Gooding J J 2014 Colloidal silicon quantum dots: from preparation to the modification of self-assembled monolayers (SAMs) for bio-applications *Chem. Soc. Rev.* **43** 2680
- [7] O'Farrell N, Houlton A and Horrocks B R 2006 Silicon nanoparticles: applications in cell biology and medicine *Int. J. Nanomed.* **1** 451–72
- [8] Lillo C R, Romero J J, Portolés M L, Diez R P, Caregnato P and Gonzalez M C 2015 Organic coating of 1–2 nm size silicon nanoparticles: effect on particle properties *Nano Res.* **8** 2047–62
- [9] Romero J J, Llansola-Portolés M J, Dell'Arciprete M L, Rodríguez H B, Moore A L and Gonzalez M C 2013 Photoluminescent 1–2 nm sized silicon nanoparticles: a surface-dependent system *Chem. Mater.* **25** 3488–98
- [10] Kango S, Kalia S, Celli A, Njuguna J, Habibi Y and Kumar R 2013 Surface modification of inorganic nanoparticles for development of organic–inorganic nanocomposites—a review *Prog. Polym. Sci.* **38** 1232–61
- [11] Storm G, Belliot S O, Daemen T and Lasic D D 1995 Surface modification of nanoparticles to oppose uptake by the mononuclear phagocyte system *Adv. Drug. Deliv. Rev.* **17** 31–48
- [12] McVey B F P and Tilley R D 2014 Solution synthesis, optical properties, and bioimaging applications of silicon nanocrystals *Acc. Chem. Res.* **47** 3045–51
- [13] Wang C-H *et al* 2008 Optimizing the size and surface properties of polyethylene glycol (PEG)–gold nanoparticles by intense x-ray irradiation *J. Phys. D: Appl. Phys.* **41** 195301
- [14] He Q *et al* 2010 The effect of PEGylation of mesoporous silica nanoparticles on nonspecific binding of serum proteins and cellular responses *Biomaterials* **31** 1085–92
- [15] Owens D E and Peppas N A 2006 Opsonization, biodistribution, and pharmacokinetics of polymeric nanoparticles *Int. J. Pharm.* **307** 93–102
- [16] Xu Z *et al* 2015 Water-soluble PEGylated silicon nanoparticles and their assembly into swellable nanoparticle aggregates *J. Nanopart. Res.* **17** 1–16
- [17] Buxadera-Palomero J, Canal C, Torrent-Camarero S, Garrido B, Javier Gil F and Rodríguez D 2015 Antifouling coatings for dental implants: polyethylene glycol-like coatings on titanium by plasma polymerization *Biointerphases* **10** 29505
- [18] Dong B, Jiang H, Manolache S, Wong A C L and Denes F S 2007 Plasma-mediated grafting of poly(ethylene glycol) on polyamide and polyester surfaces and evaluation of antifouling ability of modified substrates *Langmuir* **23** 7306–13
- [19] Xu H *et al* 2013 Characterizing pilus-mediated adhesion of biofilm-forming *E. coli* to chemically diverse surfaces using atomic force microscopy *Langmuir* **29** 3000–11
- [20] Fang B *et al* 2011 Bacterial adhesion on hybrid cationic nanoparticle–polymer brush surfaces: ionic strength tunes capture from monovalent to multivalent binding *Colloids Surf. B* **87** 109–15
- [21] Mulligan M E *et al* 1993 Methicillin-resistant *Staphylococcus aureus*: a consensus review of the microbiology, pathogenesis, and epidemiology with implications for prevention and management *Am. J. Med.* **94** 313–28
- [22] Solberg C O 2000 Spread of *Staphylococcus aureus* in hospitals: causes and prevention *Scand. J. Infect. Dis.* **32** 587–95
- [23] Lakowicz J R 2006 *Principles of Fluorescence Spectroscopy* 3rd edn (New York: Springer)
- [24] Schmidt R and Afshari E 1990 Comment on 'effect of solvent on the phosphorescence rate constant of singlet molecular oxygen' *J. Phys. Chem.* **94** 4377–8
- [25] Wilkinson F, Helman W and Ross A 1993 Quantum yields of the photosensitized formation of the lowest electronically excited singlet state of molecular oxygen in solution *J. Phys. Chem. Ref. Data* **22** 1–29
- [26] Montalti M, Credi A, Prodi L and Gandolfi M T 2006 Chemical actinometry *Handbook of Photochemistry* (Boca Raton, FL: CRC Press) pp 601–16
- [27] San Román E and Gonzalez M C 1989 Analysis of spectrally resolved kinetic data and time-resolved spectra by bilinear regression *J. Phys. Chem.* **93** 3532–6
- [28] Andrews J M 2001 Determination of minimum inhibitory concentrations *J. Antimicrobial Chemother.* **48** 5–16
- [29] Flores C Y, Miñán A G, Grillo C A, Salvarezza R C, Vericat C and Schilardi P L 2013 Citrate-capped silver nanoparticles showing good bactericidal effect against both planktonic and sessile bacteria and a low cytotoxicity to osteoblastic cells *ACS Appl. Mater. Interfaces* **5** 3149–59
- [30] Cho B, Baek S, Woo H-G and Sohn H 2014 Synthesis of silicon quantum dots showing high quantum efficiency *J. Nanosci. Nanotechnol.* **14** 5868–72
- [31] Nolan B M, Henneberger T, Waibel M, Fässler T F and Kautzlarich S M 2015 Silicon nanoparticles by the oxidation of  $[\text{Si}_4]^{4+}$ - and  $[\text{Si}_9]^{4+}$ -containing zintl phases and their corresponding yield *Inorg. Chem.* **54** 396–401

- [32] Llansola Portolés M J, Nieto F R, Soria D B, Amalvy J I, Peruzzo P J, Mártire D O, Kotler M and Oliver Holub M C G 2009 Photophysical properties of blue-emitting silicon nanoparticles *J. Phys. Chem. C* **113** 13694–702
- [33] Mallard P J L and W G 2011 NIST Chemistry WebBook, NIST Standard Reference Database Number 69 <http://webbook.nist.gov/>
- [34] Portolés M J L *et al* 2012 Understanding the parameters affecting the photoluminescence of silicon nanoparticles *J. Phys. Chem. C* **116** 11315–25
- [35] Estes M and Moddel G 1996 Luminescence from amorphous silicon nanostructures *Phys. Rev. B* **54** 14633–42
- [36] Fauchet P M 2005 Light emission from Si quantum dots *Mater. Today* **8** 26–33
- [37] Park N-M, Kim T-S and Park S-J 2001 Band gap engineering of amorphous silicon quantum dots for light-emitting diodes *Appl. Phys. Lett.* **78** 2575–7
- [38] Dohnalová K *et al* 2013 Surface brightens up Si quantum dots: direct bandgap-like size-tunable emission *Light Sci. Appl.* **2** e47
- [39] Torricelli G, Akraiam A and von Haeften K 2011 Size-selecting effect of water on fluorescent silicon clusters *Nanotechnology* **22** 315711
- [40] Dasog M, De Los Reyes G B, Titova L V, Hegmann F A and Veinot J G C 2014 Size versus surface: tuning the photoluminescence of freestanding silicon nanocrystals across the visible spectrum via surface groups *ACS Nano* **8** 9636–48
- [41] Pettigrew K A, Liu Q, Power P P and Kauzlarich S M 2003 Solution synthesis of alkyl- and alkyl/alkoxy-capped silicon nanoparticles via oxidation of Mg<sub>2</sub>Si *Chem. Mater.* **15** 4005–11
- [42] Yang J, Fang H and Gao Y 2016 Effect of water adsorption on the photoluminescence of silicon quantum dots *J. Phys. Chem. Lett.* **7** 1788–93
- [43] Liao W and Lee S 1996 Water induced room temperature oxidation of Si–H and –Si–Si– bonds in silicon oxide *J. Appl. Phys.* **80** 1171–6
- [44] Rahme K, Chen L, Hobbs R G, Morris M A, O’Driscoll C and Holmes J D 2013 PEGylated gold nanoparticles: polymer quantification as a function of PEG lengths and nanoparticle dimensions *RSC Adv.* **3** 6085–94
- [45] Fan M, Liang Y, Zhou F and Liu W 2012 Dramatically improved friction reduction and wear resistance by *in situ* formed ionic liquids *RSC Adv.* **2** 6824
- [46] Kwon H, Lim E, Lee S and Lee K K 2014 Synthesis and characterization of poly(vinylpyrrolidone)-capped silicon nanoparticles *J. Nanosci. Nanotechnol.* **14** 5983–7
- [47] Chen D, Yi R, Chen S, Xu T, Gordin M L and Wang D 2014 Facile synthesis of graphene-silicon nanocomposites with an advanced binder for high-performance lithium-ion battery anodes *Solid State Ion.* **254** 65–71
- [48] Lee H, Venable R M, Mackerell A D and Pastor R W 2008 Molecular dynamics studies of polyethylene oxide and polyethylene glycol: hydrodynamic radius and shape anisotropy *Biophys. J.* **95** 1590–9
- [49] Oelmeier S A, Dismar F and Hubbuch J 2012 Molecular dynamics simulations on aqueous two-phase systems—single PEG-molecules in solution *BMC Biophys.* **5** 14
- [50] Ling K, Jiang H and Zhang Q 2013 A colorimetric method for the molecular weight determination of polyethylene glycol using gold nanoparticles *Nanoscale Res. Lett.* **8** 538
- [51] Schweitzer C and Schmidt R 2003 Physical mechanisms of generation and deactivation of singlet oxygen *Chem. Rev.* **103** 1685–757
- [52] Kim S, Fujitsuka M and Majima T 2013 Photochemistry of singlet oxygen sensor green *J. Phys. Chem. B* **117** 13985–92
- [53] Rota C, Chignell C F and Mason R P 1999 Evidence for free radical formation during the oxidation of 2'-7'-dichlorofluorescein to the fluorescent dye 2'-7'-dichlorofluorescein by horseradish peroxidase: possible implications for oxidative stress measurements *Free Radical Biol. Med.* **27** 873–81
- [54] Lambrechts S A G, Demidova T N, Aalders M C G, Hasan T and Hamblin M R 2005 Photodynamic therapy for *Staphylococcus aureus* infected burn wounds in mice *Photochem. Photobiol. Sci.* **4** 503–9